FORSCHUNGSZENTRUM ROSSENDORF FZR

FZR-191
August 1997
Preprint

V.V. Shklyar, B. Kämpfer, B.L. Reznik and A.I. Titov

Bremsstrahlung in intermediate-energy nucleon reactions within an effective one-boson exchange model

Herausgeber:
FORSCHUNGSZENTRUM ROSSENDORF
Postfach 51 01 19
D-01314 Dresden
Telefon (03 51) 26 00
Telefax (03 51) 2 69 04 61

Als Manuskript gedruckt

Bremsstrahlung in intermediate-energy nucleon reactions within an effective one-boson exchange model

V.V. SHKLYAR[a,b], B. KÄMPFER[c], B.L. REZNIK[b], A.I. TITOV[a,b]

[a] *Bogoliubov Theoretical Laboratory, Joint Institute for Nuclear Research, 141980 Dubna, Russia*

[b] *Far-Eastern State University, Sukhanova str. 8, Vladivostok 690900, Russia*

[c] *Research Center Rossendorf Inc., Institute for Nuclear and Hadron Physics, PF 510119, 01314 Dresden, Germany*

Abstract

Within a covariant effective one-boson exchange model for the T matrix of NN interactions we present detailed calculations of bremsstrahlung cross sections for proton - proton and proton - neutron reactions at beam energies in the 1 GeV region. Besides pure bremsstrahlung processes we consider photons from Δ decays and contributions from the $\eta \to \gamma\gamma$ process. At beam energies above 700 MeV the Δ decay channel dominates the spectra at large photon energies, where the interference between non-resonance processes and the Δ decay channel becomes also important. Low energy photons stem from pure bremsstrahlung processes. The available experimental data at 730 MeV beam energy is well described. We extrapolate the model down to 280 MeV, where more detailed experimental data exist, and find agreement with angular distributions.

Key Words: bremsstrahlung, effective one-boson exchange model

PACS: 13.75.Cs, 25.20.-x, 25.40.-h

I. INTRODUCTION

The series of experiments with proton kinetic energies $T_{\rm kin}$ = 280 - 2500 MeV at the new cooler synchrotron (COSY) in Jülich promises a wealth of precision data of various hadronic reactions. Among the particle production experiments a systematic study of bremsstrahlung processes is envisaged [1], and the first data with the time-of-flight detector system TOF are analyzed [2]. The interest in bremsstrahlung is as usual for electromagnetic processes in strongly interacting systems: real or virtual photons serve as clean probes of the strong interaction.

In the energy region up to the pion production threshold at beam energy of $T_{\rm kin} \simeq 280$ MeV the bremsstrahlung can test the half-off-shell part of the nucleon - nucleon (NN) potential. One motivation for such experiments was therefore to constrain the various potential models of the low-energy NN interaction. Recent studies [3–5] however show that several bremsstrahlung observables are not too sensitive to different parametrizations of the NN potential. New precision data might allow for some progress, since the available data set in this energy region [6,7], as noted in Refs. [4,5,8,9], does not point to a preferable NN potential. Indeed, various models can account for the data [5,8,10], even if there is some uncertainty concerning the absolute normalization of the cross section [7]. Some new possibilities to distinguish among various potential approaches in bremsstrahlung reactions are proposed recently in Ref. [11].

At higher beam energy there is only one data set available, namely at $T_{\rm kin}$ = 730 MeV [12] where the energy spectrum of the outgoing photons in limited phase space regions has been measured. This data has been analyzed early [13] and also recently in Ref. [5] within covariant models based on π and ρ exchanges. At COSY the measurements can be extended in a broad beam energy interval up to 2.5 GeV and deliver angular distributions of photons and recoil nucleons. Theoretically, one must utilize appropriate covariant strong interaction models in this energy region.

In particular the covariant one-boson exchange (OBE) models represent a powerful tool for describing hadron reactions in the GeV region. Such models have been employed for analyzing [14–17] the virtual photon (i.e., di-electron) production [18]. Recently, also the OBE description of pion production finds renewed interest [19]. Therefore, it seems worthwhile to apply the same model to the real photon production processes to arrive at a coherent picture of electromagnetic processes in strong interactions of nucleons. Such a task is particularly tempting as there are controversial explanations of peculiarities of the virtual photon production mechanism at $T_{\rm kin}$ = 1 - 1.5 GeV [14,15,17]: Either subtle interferences between non-resonance and resonance (including the Δ) channels or a strong contribution of η Dalitz decays can explain the non-trivial beam energy dependence of cross sections. Measurements of refined observables [20] might disentangle the various di-electron sources. On the other hand an independent test of real photon production in the mentioned energy region may be important for studying this problem as well.

Here we present results of detailed calculations of the real photon bremsstrahlung within a relativistic and gauge-invariant effective OBE model, which continues and extends earlier investigations [15,21–23] for the reaction $NN \to NN\gamma$. We go beyond our previous study [23] by including the internal radiative meson conversions, the anomalous magnetic moment of the nucleons, and a wider beam energy interval. Conceptually, our approach is close to the model of Ref. [17]. The main difference rests in a different goal of our study: We here consider angular and energy distributions of real photons instead of inclusive invariant

mass distributions of di-electrons as in Ref. [17]. Additionally we employ a slightly different prescription for the Δ excitation vertex and effective parameters in the two-body elastic scattering T matrix. In relation to Ref. [5] where only π, ρ exchange has been considered, we include the exchange of σ and ω mesons as well and we take into account radiation from internal lines with vector mesons $V = \rho, \omega$ in $V\pi\gamma$ vertices.

Our paper is organized as follows. In Section 2, we formulate our effective OBE model approach for non-resonance and resonance contributions to the reaction $NN \to NN\gamma$. Concerning the resonance contributions we restrict our consideration to the implementation of the Δ excitation and decay channel. In Section 3 we analyze contributions of different channels in the 1 GeV region and present a comparison with the available experimental data for $pp \to pp\gamma$ at beam energy of 730 MeV. In Section 4 we discuss the contribution of the $\eta \to \gamma\gamma$ decay channel to the $NN \to X\gamma$ reaction and compare it with the strongly interfering Δ decay process and non-resonance bremsstrahlung channels. In Section 5 we compare our model with data at 280 MeV and discuss whether the effective two-body T matrix model may be applied here. The summary is given in Section 6. In the present paper we restrict ourselves to unpolarized observables. The analysis of polarization effects in NN bremsstrahlung will be subject of a forthcoming paper.

II. $NN \to NN\gamma$ BREMSSTRAHLUNG

The differential cross section of the exclusive reaction $N_1N_2 \to N_1'N_2'\gamma$ reads in a Fermion - Boson symmetric convention

$$d\sigma(\sqrt{s}) = \frac{1}{2(2\pi)^5\sqrt{s(s-4M_N^2)}}\,|\overline{\mathcal{M}}|^2\,\frac{d\mathbf{p}_1'}{2E_1'}\,\frac{d\mathbf{p}_2'}{2E_2'}\,\frac{d\mathbf{k}}{2\omega}\,\delta^{(4)}(p_1+p_2-p_1'-p_2'-k), \tag{1}$$

where $k = (\omega, \mathbf{k})$ denotes the four vector of the outgoing photon, $p_{1,2} = (E_{1,2}, \mathbf{p}_{1,2})$ and $p'_{1,2} = (E'_{1,2}, \mathbf{p'}_{1,2})$ are initial and final nucleon four-momenta, respectively. $\sqrt{s}$ is the total available energy, and the nucleon mass is denoted by M_N.

We do not consider here polarization observables, therefore the matrix element $|\overline{\mathcal{M}}|^2$ is spin averaged in the entrance channel and spin summed in the exit channel. By partially integrating over energies and directions of the outgoing particles one arrives at experimentally relevant quantities, e.g., $d\sigma/d\omega d\Omega_\gamma d\Omega_{p'}$ where ω stands for the photon energy in the center-of-mass system (cms), and Ω_γ and $\Omega_{p'}$ denote the cms angles of outgoing particles. This differential cross section can be written as

$$\frac{\omega d^5\sigma}{d\omega\, d\Omega_\gamma d\Omega_{p'}} = \frac{\omega^2}{8\,(2\pi)^5\sqrt{s\,(s-4M_N^2)}}\,|\overline{\mathcal{M}}|^2\,D(p'), \tag{2}$$

where

$$D(p') = \frac{p'^2}{|Ap' + CE'|}, \tag{3}$$

with

$$E' = \frac{AB - C\sqrt{B^2 - M_N^2(A^2-C^2)}}{A^2-C^2},$$
$$A = 2(\sqrt{s}-\omega),\quad B = s - 2\omega\sqrt{s},\quad C = 2\omega\cos\Theta_{\mathbf{p'k}}.$$

The 3-momentum of the outgoing proton in the cms is $\mathbf{p}'$ with $p'^2 = \mathbf{p}'^2 = E'^2 - M_N^2$.

We perform diagrammatic calculations of bremsstrahlung processes on the basis of the OBE model, where four exchanged mesons $M = \pi^{\pm,0}, \rho^{\pm,0}, \omega, \sigma$ are used for the description of the two-body pp and pn T matrices. The resulting elementary Feynman diagrams which contribute to the amplitude $\mathcal{M}$ are displayed in Fig. 1. Let us first consider the pp reaction. The amplitude

$$^{pp}\mathcal{M} = \sum_{M=\pi^0,\sigma,\omega,\rho^0} {}^{pp}\hat{\mathcal{M}}_M^{(1)} + \sum_{MM'=V^0,\pi^0} {}^{pp}\hat{\mathcal{M}}_{MM'}^{(2)} + \sum_{M=\pi^0,\rho^0} {}^{pp}\hat{\mathcal{M}}_M^{(3)} \tag{4}$$

is a coherent sum of (i) pure bremsstrahlung diagrams ${}^{pp}\hat{\mathcal{M}}_M^{(1)}$ with pre-emission and post-emission of a photon with momentum k as shown in Figs. 1a - d, where the intermediate nucleon is an off-shell proton, (ii) the contributions from internal radiative meson conversions ${}^{pp}\hat{\mathcal{M}}_{MM'}^{(2)}$ according to the processes $V^0 \to \pi^0\gamma$ (where V^0=ρ^0, ω) displayed in Fig. 1f, and (iii) resonance contributions ${}^{pp}\hat{\mathcal{M}}_M^{(3)}$ from excitation and decay of the $\Delta^+(1232)$ resonance as depicted in Figs. 1a - d. In (ii) we neglect possible $V \to \eta\gamma$ transitions because the corresponding coupling constants are expected to be negligible small [24]. Due to identical particles in the initial and exit channel the corresponding exchange diagrams must be included, i.e.,

$${}^{pp}\hat{\mathcal{M}}_{\cdots}^{(n)} = {}^{pp}\mathcal{M}_{\cdots}^{(n)}(p_1, p_2; p_1', p_2') - {}^{pp}\mathcal{M}_{\cdots}^{(n)}(p_1, p_2; p_2', p_1'), \quad n = 1, \cdots, 3.$$

This results in a total of 48 diagrams, i.e., 32 pure bremsstrahlung contributions, 8 graphs with Δ excitation, and 8 diagrams with internal meson conversion.

The matrix element for the reaction $pn \to pn\gamma$ reads accordingly

$$\begin{aligned} ^{pn}\mathcal{M} = &\sum_{M=\pi^0,\sigma,\omega,\rho^0} {}^{pn}\mathcal{M}_M^{(1)} + \sum_{M=\pi^\pm,\rho^\pm} {}^{pn}\mathcal{M}_M^{(2)} + \sum_{M=\rho^\pm,\pi^\pm} {}^{pn}\mathcal{M}_M^{(3)} \\ &+ \sum_{MM'=V,\pi} {}^{pn}\mathcal{M}_{MM'}^{(4)} + \sum_{M=\pi^0,\rho^0} {}^{pn}\mathcal{M}_M^{(5)} + \sum_{M=\pi^\pm,\rho^\pm} {}^{pn}\mathcal{M}_M^{(6)} \end{aligned} \tag{5}$$

and contains the pure bremsstrahlung processes with exchange of neutral and charged mesons ${}^{pn}\mathcal{M}_M^{(1,2)}$ (Figs. 1a - d), radiation from charged internal mesons ${}^{pn}\mathcal{M}_M^{(3)}$ (Fig. 1e), internal radiative meson conversion ${}^{pn}\mathcal{M}_{MM'}^{(4)}$ (Fig. 1f), and resonance contributions from the $\Delta^{+,0}$ decays ${}^{pn}\mathcal{M}_M^{(5,6)}$ (Figs. 1a - d). This yields 36 diagrams in total, i.e., 24 pure bremsstrahlung contributions, 6 graphs with Δ excitation, and 8 diagrams with internal meson conversion. The contributions from the inclusive processes depicted in Figs. 1g and h in pp and pn reactions will be separately discussed in Section 3.

A. Non-resonance pure bremsstrahlung

To evaluate the mentioned matrix elements we employ the covariant perturbation theory in first order to nucleon - nucleon interactions. The nucleon - meson interaction Lagrangian reads in obvious standard notation

$$\mathcal{L}_{int} = -ig_\pi\bar{\psi}\gamma_5\boldsymbol{\tau}\psi\boldsymbol{\pi} + g_\rho\bar{\psi}\gamma_\mu\boldsymbol{\tau}\psi\boldsymbol{\rho}^\mu + g_\omega\bar{\psi}\gamma_\mu\psi\omega^\mu + g_\sigma\bar{\psi}\psi\sigma, \tag{6}$$

where ψ represents the nucleon bispinor, and π, $\boldsymbol{\rho}_\mu$, ω_μ, σ stand for the respective meson fields; $\mu, \nu \cdots$ are used as Lorentz indices, and $\boldsymbol{\tau}$ is the Pauli matrix. Symbols in boldface denote here isovectors. Note that we employ the pseudo-scalar πNN coupling. It is known that the pseudo-vector and pseudo-scalar couplings give analogous results on the tree amplitude level [22].

The strong NNM vertices are dressed by monopole form factors: either for each vertex

$$F_{NNM}(q^2) = \frac{\Lambda_M^2 - m_M^2}{\Lambda_M^2 - q^2}, \tag{7}$$

when the internal meson line carries the momentum q, or for both vertices

$$F_{NNM}(q_1^2) F_{NNM'}(q_2^2) \left(1 + \frac{m_M^2 - q_1^2}{\Lambda_M^2 - q_2^2} + \frac{m_M^2 - q_2^2}{\Lambda_M^2 - q_1^2}\right), \tag{8}$$

when the internal line radiates a photon with momentum $k = \pm(q_1 - q_2)$; the $MM'\gamma$ vertex is then

$$\Gamma^\mu_{MM\gamma} = -ie(q_1 + q_2)^\mu, \tag{9}$$

with e as electromagnetic coupling. If the photon is emitted from a nucleon line the $NN\gamma$ vertex function is as usual

$$\Gamma^\mu_{\gamma NN}(p', p) = -ie\left[\gamma^\mu F_1 + i\frac{\kappa_N}{2M_N}\sigma^{\mu\nu}(p'_\nu - p_\nu)F_2\right], \tag{10}$$

where κ_N is the anomalous magnetic nucleon moment ($\kappa = 1.79$ for protons and -1.91 for neutrons) in terms of the nuclear magneton, and $F_{1,2} = 1$ for protons and $F_1 = 0$, $F_2 = 1$ for neutrons. The form factors are constructed in such a way that they preserve gauge invariance [17,25,26].

For the elastic NN scattering, the strong NNM vertex form factor (7) depends only on the momentum transfer squared q^2. For the half-off-shell T matrix, which appears in the bremsstrahlung processes, the effective vertex functions, in general, must depend on an additional invariant variable. The momentum squared p^2 of the off-shell nucleon may be chosen as such a variable. A procedure of including the off-shell dependence into both the electromagnetic form factors $F_{1,2}$ and two-body T matrices is discussed in Ref. [17], and it is argued that the off-shell correction is expected to be not so large. In order to avoid in the present consideration poorly constrained additional parameters, we assume that the above adjusted on-shell T matrix parameters are applicable also for the half-off-shell amplitudes. In this respect the below presented calculations might be considered as an upper bound of the non-resonance bremsstrahlung contribution since off-shell corrections usually suppress form factors.

In our calculations we use energy dependent parametrizations of the elastic pp and pn scattering, where the effective coupling constants g_M change with beam energy according to $g_M(s) = g_M^0 \exp(-\beta_M\sqrt{s - 4M_N^2})$ [27]. The meson masses m_M, coupling strengths g_M, and cut-off parameters Λ_M are adjusted by standard fits to the known experimental data and are listed in Table 1 together with the energy parameter β_M. In Fig. 2 we show the results of our calculations for the elastic NN scattering in comparison with experimental data [28,30] at two relevant beam energies.

Together with the conventional photon radiation from the charged exchange meson lines we include the radiation from internal radiative decays as described above. The corresponding decay vertex reads

$$\Gamma^{\nu\beta}_{V\pi\gamma} = -ig_{V\pi\gamma}\epsilon^{\mu\nu\alpha\beta}k_\alpha q_\mu, \tag{11}$$

where V denotes the vector mesons ω and ρ, and q and k are the pion and photon momenta; $\epsilon^{\mu\nu\alpha\beta}$ is the Levi-Civita symbol. The coupling constants $g_{V\pi\gamma}$ are adjusted to the experimental $V \to \pi\gamma$ decay widths [24]. Their numerical values are

$$\frac{g^2_{\omega\pi\gamma}}{4\pi} = 3.94\cdot 10^{-2}\,\mathrm{GeV}^{-2},\ \frac{g^2_{\rho^0\pi^0\gamma}}{4\pi} = 0.692\cdot 10^{-2}\,\mathrm{GeV}^{-2},\ \frac{g^2_{\rho^\pm\pi^\pm\gamma}}{4\pi} = 0.396\cdot 10^{-2}\,\mathrm{GeV}^{-2}. \tag{12}$$

The choice of a positive sign for the $\omega\pi\gamma$ amplitude and a negative sign for $\rho\pi\gamma$ is consistent with the data on pion photoproduction [29]. The NNV vertices in $V\pi\gamma$ decay diagrams are the same as discussed above for the conventional OBE amplitudes with the same form factors and energy dependence of the coupling constants.

B. Δ excitation in NN bremsstrahlung

A second subgroup of contributions to $NN \to NN\gamma$ bremsstrahlung contains the excitation of $\Delta^{+,0}$ and the subsequent decay $\Delta \to N\gamma$ according to the diagrams in Figs. 1a - d. The isospin $\frac{3}{2}$ of the Δ requires the coupling to the isovectors π and ρ in the corresponding vertices. The parameters of the $\Delta N\pi$ and $\Delta N\rho$ vertices are adjusted by fitting both the calculated Δ production cross section and the $\Delta \to N\pi$ angular distribution to experimental data. Unfortunately, these data do not allow for a unique set of parameters for both $\Delta N\pi$ and $\Delta N\rho$ vertices. One of the possible sets even does not need a ρ exchange contribution [15]. This is consistent with the parametrization of Ref. [17], where the relative amplitude of the ρ exchange is about one order of magnitude smaller than that for the π exchange, i.e.,

$$\frac{T_\rho}{T_\pi} \sim \frac{f_{N\Delta\rho}}{f_{N\Delta\pi}}\frac{m_\pi}{m_\rho}\frac{\sqrt{g^2_{NN\rho}}}{\sqrt{g^2_{NN\pi}}} \simeq 0.1. \tag{13}$$

Moreover, this ratio T_ρ/T_π decreases if form factors with cut-off parameters are included. Relying on this fact and trying to use in our calculations as few as possible parameters, we restrict ourselves in this subsection to resonance excitation via π exchange alone.

The $NN \to N\Delta$ interaction is characterized by the amplitude

$$\mathcal{T}^\Delta = g_\Delta\, F^2_\Delta(q^2)(\bar\psi^\Delta_\mu \boldsymbol{T} q^\mu \psi)(\bar\psi\boldsymbol{\tau}\gamma_5\psi)\,(m^2_\pi - q^2)^{-1}, \tag{14}$$

where the form factor F_Δ has the same form as in Eq. (7) but now with the cut-off Λ_Δ. The isospin transition operator $\mathbf{T}$ is defined as in Ref. [36]. The propagator of the Δ is used in the standard form for Rarita - Schwinger fields

$$S^{\mu\nu}_\Delta(p) = \frac{-(\gamma^\alpha p_\alpha + M_\Delta)}{(p^2 - M^2_\Delta + iM_\Delta\,\Gamma_\Delta(p^2))}[g^{\mu\nu} - \frac{1}{3}\gamma^\mu\gamma^\nu - \frac{2}{3}M_\Delta^{-2}p^\mu p^\nu - \frac{1}{3}M_\Delta^{-1}(\gamma^\mu p^\nu - p^\mu\gamma^\nu)], \tag{15}$$

with $M_\Delta = 1.232$ GeV and momentum dependent width $\Gamma_\Delta(p^2)$ as in Ref. [31]

$$\Gamma_\Delta(p^2) = \Gamma^0_\Delta \left[\frac{k(p^2)}{k(M^2_\Delta)}\right]^3 \frac{k^2(M^2_\Delta)+c^2}{k^2(p^2)+c^2}, \quad c = 200\text{MeV}, \tag{16}$$

$$k(p^2) = \sqrt{\frac{(p^2+M^2_N-m^2_\pi)^2}{4p^2} - M^2_N}. \tag{17}$$

The effective strength parameter g_Δ in Eq. (14) is normalized to the VerWest - Arndt parametrization of the total Δ production cross section σ^{WA}_Δ [32]

$$g^2_\Delta = \frac{\sigma^{WA}_\Delta}{\int dt\,(d\sigma_\Delta/dt)}, \tag{18}$$

where the angular differential cross section

$$\frac{d\sigma_\Delta}{dt} = \frac{1}{16\pi s(s-4M^2_N)}\,|\bar{T}^\Delta|^2 \tag{19}$$

is calculated within our model with direct and exchange terms. The cut-off parameter $\Lambda_\Delta = 0.7$ GeV is fixed by the requirement to get a optimum reproduction of the experimental data on the Δ production angular distribution [33], see Fig. 1 in Ref. [15].

Finally, the decay vertex $\Delta \to N\gamma$ is parametrized by

$$\Gamma_{\mu\alpha} = -ieG_\Delta(\gamma^\nu k_\nu g_{\mu\alpha} - \gamma_\alpha k_\mu)\gamma_5 \tag{20}$$

with $G_\Delta = 2.18$, which results in the decay width $\Gamma^{\Delta\to N\gamma} = \tilde{B}^{\Delta\to N\gamma}\Gamma^0_\Delta$, where $\tilde{B}^{\Delta\to N\gamma} = 6\cdot 10^{-2}$ is the branching ratio, and $\Gamma^0_\Delta = 0.12$ GeV denotes the total Δ width.

III. RESULTS OF BREMSSTRAHLUNG CALCULATIONS

Now we are going to present the results of our numerical calculations of the above cross sections. Let us first consider the contribution of the anomalous magnetic moment of the nucleon in the vertex Eq. (10) at T_{kin}=1 GeV. For the sake of simplicity we show in Fig. 3 the triple differential cross section $\omega d^3\sigma/d\omega\, d\Omega_\gamma$ at fixed angle of the outgoing photon. The contribution of the anomalous moment is proportional to ω^4 and becomes important at relatively large photon energies, i.e., at $\omega > \omega_{\text{max}}/2$, where $\omega_{\text{max}} = (s-4M^2_N)/2\sqrt{s}$. At low photon energies only the electric part of the electromagnetic current contributes, and the cross section is well described by the conventional soft-photon approximation. The relative effect of the anomalous magnetic moment in pp scattering is larger than in pn interactions.

The magnetic structure of the vertex in Eq. (11) leads to a similar behavior of the contribution from the internal $V \to \pi\gamma$ transition, but its absolute value is much smaller in the 1 GeV region as shown in Fig. 4. This figure is more of methodical interest because at initial energy above the Δ production threshold and at $\omega > 0.2$ - $0.4\ \omega_{\text{max}}$, the contribution of the Δ channel becomes anyhow dominant. Below the Δ threshold the $\omega/\rho \to \pi\gamma$ emission has the same order of magnitude as the magnetic terms in the non-resonance bremsstrahlung.

We have checked that the internal radiative meson conversion and the anomalous magnetic moment of the nucleons do not change, on a visible level, our previous results [23] on the differential cross sections $d\sigma/d\omega$ and $d\sigma/d\Omega_\gamma$. Therefore we are going to discuss the

cross sections for more specific geometries which are easily accessible at COSY-TOF. In particular, we select a non-coplanar geometry. Our results of the differential cross sections $\omega d^5\sigma/d\omega\, d\Omega_\gamma d\Omega_{p'}$ are displayed in Figs. 5 and 6 for pn and pp reactions at beam energies of $T_{\rm kin} = 0.7$, 1.0, 1.35 and 1.7 GeV and fixed angles in the cms. This energy interval covers the expected range of validity of our model. With increasing beam energy the rôle of Δ excitations becomes more important.

Let us first consider the reaction $pn \to pn\gamma$ in more detail. In Fig. 5a one can distinguish two regions in the energy distribution of the differential cross section. At low photon energies the pure bremsstrahlung dominates, while above $\omega/\omega_{\rm max} = 0.4$ - 0.5 most photons stem from the Δ decays. Interference effects are not important in these spectra when considering the total yield. The situation, however, changes when considering the angular distribution at $T_{\rm kin} = 700$ MeV for $\omega/\omega_{\rm max} = 0.5$ (Fig. 5b). Here the interference terms become as large as the dominating individual contributions at large angles. (Note that in Ref. [17] the strongest interference effects are also found near the kinematical boundary.) Since we keep $\omega/\omega_{\rm max} \approx 0.5$, this effect is not seen for higher bombarding energies because the value of $\omega/\omega_{\rm max}$, where the bremsstrahlung and Δ contributions are equally strong, is changed to smaller numbers.

Similar conclusions hold for the reaction $pp \to pp\gamma$ (see Fig. 6). Here the cross over in Fig. 6a from the bremsstrahlung to the Δ decay dominated region is sharper. Interference terms are smaller than the dominating contributions. The most remarkable fact is the double-humped bremsstrahlung spectrum in the angular distribution in Fig. 6b, which however is hidden under the Δ decay contribution. The relative sign of the Δ decay - bremsstrahlung interference still remains unknown. This problem was also explored in Ref. [17] for di-lepton production spectra. As illustrated in Fig. 6b, the sign of Δ decay - bremsstrahlung interference may be very important at certain photon angels at higher beam energies. In our consideration the interference term is positive at small photon angles and low beam energies, but at large photon angle and $T_{\rm kin} = 1.7$ GeV its sign changes and becomes negative. The total angular distributions in Figs. 5 and 6 do not show drastic variations, and it seems difficult to disentangle the different photon sources with these observables.

An interesting observation comes from the ratio of the photon emission cross sections for pn to pp reactions displayed in Fig. 7. From Figs. 4 and 5 alone one can hardly make a distinction between pn and pp bremsstrahlung. They have similar shapes with respect to the photon energy distribution. But one can see from Figs. 7a and b that these reactions may show quite substantial (and measurable) differences. As known, the ratio of the di-electron cross sections for pd to pp reactions up to 1.5 GeV has a non-monotonic behavior [18]. The Figs. 7a and b show that the ratio of bremsstrahlung cross sections pn/pp has an analogous shape. At large photon energy the bremsstrahlung pn/pp ratio increases similar as the di-electron ratio pd/pp does, see Fig. 7a. It is also interesting to look on the photon angular distribution in Fig. 7b. Here we predict a pronounced non-monotonic behavior of this observable at $T_{\rm kin} = 1.3$ - 1.7 GeV which stems from the large contribution of the negative Δ decay - bremsstrahlung interference term (cf. Fig. 6b).

Our results of the differential cross section $\omega d\sigma/d\omega d\Omega_\gamma d\Omega_{p'}$ might be compared with the existing experimental data on $pp \to pp\gamma$ at $T_{\rm kin} = 730$ MeV [12]. One observes in Fig. 8 a good agreement of our model (without efficiency corrections) with the raw data [12] for the counters G07 and G10. At very small photon energies one recovers the results of the soft photon approximation. At $\omega > 100$ MeV the Δ contribution becomes dominant which causes an increase of the cross section, in fair agreement with the data. This has been

already observed in Ref. [5].

IV. THE $\eta \to \gamma\gamma$ CONTRIBUTION

As mentioned in the Introduction the η meson production and its radiative two-photon decay plays an essential rôle in the di-electron spectra at 1 GeV beam energy and above [15]. In this section we estimate the η contributions to the inclusive $NN \to X\gamma$ reaction by integrating over the momentum of the second photon. This consideration has rather methodical character, because if one looks at the inclusive one-photon distribution from intermediate pseudo-scalar meson decay into two photons, one should also consider the process $\pi^0 \to \gamma\gamma$ as well, which is expected to give a rather large contribution because of the large pion production cross section. In the di-electron spectra at 1 GeV beam energy this problem does not appear since the contributions of $\pi^0 \to \gamma^*\gamma$ and $\eta \to \gamma^*\gamma$ (where γ^* is virtual photon with invariant mass $M^2 > 0$) are separated, because the π^0 decay contributes only at small invariant mass $M^2 < m_\pi^2$. But the η decay contribution may become important and may be as large as the dominant Δ decay contribution or even larger [34]. Here, we intent to study the η decay contribution in comparison with the Δ channel and the interference contribution from Δ decay and non-resonance NN bremsstrahlung as an additional independent test of the strong effect of the η Dalitz decay channel near the threshold. In doing so we assume that photons from π^0 decays need not to be considered, since they can be identified and rejected experimentally [12].

Relying on the fact that the $\eta \to \gamma\gamma$ decay width is rather small, we get the following expression for the η contribution to the triple differential cross section

$$\frac{d\sigma}{d\omega\, d\Omega} = \frac{\omega \tilde{B}^{\eta\to\gamma\gamma}\, \sigma_\eta(s)}{8\,(2\pi)^6 \sqrt{s\,(s-4M_N^2)}} \left[\frac{\int d\Omega_{p'}\, d\varphi_\eta \int\limits_{E_{\min}(\omega)}^{E_{\max}} |\overline{\mathcal{M}_\eta}|^2 D(p')\, dE_\eta}{\int d\Omega_{p'}\, d\Omega_\eta \int\limits_{m_\eta}^{E_{\max}} |\overline{\mathcal{M}_\eta}|^2 D(p')\, p_\eta\, dE_\eta} \right], \tag{21}$$

where $\sigma_\eta(s)$ is the η production cross section; $E_{\min,\max}$ are the minimum and maximum values of the η meson energy which depend on the photon energy via

$$E_{\max} = (s + m_\eta^2 - 4M_N^2)/(2\sqrt{s}), \;\; E_{\min}(\omega) = \omega + m_\eta^2/(4\omega),$$

and $D(p')$ and E' are defined as in Eq. (3), but now with

$$A = 2(\sqrt{s} - E_\eta), \;\; B = s - 2\sqrt{s}E_\eta + m_\eta^2, \;\; C = 2p_\eta \cos\Theta_{\vec{p}_\eta \vec{p}'}. \tag{22}$$

We use the known branching ratio $\tilde{B}^{\eta\to\gamma\gamma} = 0.39$. When considering the amplitudes for the process $NN \to NN\eta$ we assume that the excitation and the decay of the N_{1535} resonance dominates the η production. We calculate the N_{1535} excitation within the OBE model with $\pi^{\pm,0}, \rho^{\pm,0}, \omega, \sigma$ exchange which contribute to the matrix elements according to the post-emission diagrams in Figs. 1g and h

$$^{NN}\mathcal{M}_\eta = \sum_{M=\pi,\rho,\omega,\sigma} {}^{NN}\hat{\mathcal{M}}_M^{(g,h)},$$

where for pp reactions only the exchange of neutral mesons needs to be considered, whereas for the pn reaction also the exchange of charged mesons is included. Note that the pre-emission contributions are considerably smaller and can be neglected.

The matrix elements are constructed according to the interaction Lagrangian

$$\mathcal{L}'_{int} = -ig^*_\pi \bar{\psi}_* \boldsymbol{\tau} \psi \boldsymbol{\pi} + g^*_\rho \bar{\psi}_* \gamma_5 \gamma_\mu \boldsymbol{\tau} \psi \boldsymbol{\rho}^\mu + g^*_\omega \bar{\psi}_* \gamma_5 \gamma_\mu \psi \omega^\mu + g^*_\sigma \bar{\psi}_* \gamma_5 \psi \sigma + g^*_\eta \bar{\psi}_* \psi \eta, \tag{23}$$

where ψ_* denotes the N_{1535} wave function and $g^*_M = g^{*0}_M F_M$ are the corresponding coupling constants with the same form factors according to Eq. (7) as in NNM vertices. Evaluating the η production cross section we use same procedure as in the Δ production, i.e., the normalization of $\sigma_\eta(s)$ to the known experimental value. In our calculations we employ the parametrization

$$\sigma_\eta = \frac{a\,(1-\xi^2)}{(1+[b(\xi^{-1}-1)]^c)\sqrt{s(s-4M_N^2)}}, \tag{24}$$

with $a = 4 \cdot 10^2$ $(3 \cdot 10^3)$ mb·GeV^2, $b = 17$ (33) and $c = 1.8$ (2.1) for pp (pn) reactions. The quantity ξ is defined as $\xi = \sqrt{s_0/s}$ with $s_0 = (2M_N + m_\eta)^2$. This parametrization is in agreement with results of Ref. [27] and numerically coincides with Ref. [35] and has been used for di-electron production [15]. Eq. (24) allows to constrain one parameter in the set of coupling constants, and as a result we need only the ratios of $g^{*0}_\pi : g^{*0}_\rho : g^{*0}_\omega : g^{*0}_\sigma = 1 : 0.78 : 0.55 : 0.17$ which are taken from Ref. [27].

Eq. (21) shows that the η decay contributes in the window $\tilde{\omega}_{\min} \le \omega \le \tilde{\omega}_{\max}$ with $\tilde{\omega}^{\max}_{\min} = \frac{1}{2}(E_{\max} \pm \sqrt{E^2_{\max} - m^2_\eta})$. The N_{1535} resonance is assumed to be an unstable particle, which can be described by replacing $M_N \to M^* - i\frac{1}{2}\Gamma^*$ in the nucleon propagator with $M^* = 1535$ MeV and $\Gamma^* = 180$ MeV.

Our results are displayed in Figs. 9a and b for pn and pp collisions at $T_{\rm kin}$ =1.35 and 1.7 GeV. The energy $T_{\rm kin} = 1.35$ GeV is just slightly above the η threshold. At $T_{\rm kin} = 1.7$ GeV there is a narrow window wherein the η decay contribution almost shines out. Within this window the η channel is as large as the dominant Δ decay contribution, which is in agreement with previous conclusions [14]. However, at extremely large photon energies $\omega \to \omega_{\max}$ the interference of the Δ channel with the pure bremsstrahlung process becomes comparable with the dominant channel. That is again in agreement with previous findings [17]. So we conclude that for a clear understanding of the inclusive real and virtual photon spectra both η decay and strong interference of the resonance and non-resonance bremsstrahlung must be taken into account especially for photon energies close to the kinematical limit.

V. NN BREMSSTRAHLUNG AT $T_{\rm KIN} = 280$ MEV

As mentioned in the Introduction, there is a large body of experimental data on NN bremsstrahlung at beam energies $T_{\rm kin} \sim 200$ - 300 MeV around the pion production threshold, and new precision data are to be expected soon from COSY-TOF and other installations. Therefore, it seems interesting to check a possible applicability of the OBE model by comparing with this data. One should stress, however, that the more elaborate potential models are usually considered as adequate in this energy region, since initial and final state interaction effects may be essential. However, there is no standard potential model. Various groups suggest their own models with specific approximations. That makes a comparison between different approaches rather difficult. We mention in this context also a recent successful application of the effective OBE model to a description of meson production in a wide energy interval down to the pion threshold [19]. All this inspires us to apply our effective OBE

model to the low energy bremsstrahlung data. Note that it is not obvious that the effective two-body T matrix with parameters adjusted at much higher energies is adequate for such low energy NN scattering. Nevertheless, we expect that the OBE model reproduces the cross features of bremsstrahlung in this energy region.

We calculate the differential cross section $d^5\sigma/d\Omega_{p_1'}d\Omega_{p_2'}d\vartheta_\gamma$ for bremsstrahlung as a function of the photon polar angle ϑ_γ at fixed polar proton angles $\vartheta_{p_{1',2'}}$ at $T_{\rm kin} = 280$ MeV. A comparison of our results with the data [7] are shown in Fig. 10. One can see that the OBE model describes, without any fine tuning of the parameters, the structure of the data quite satisfactory. Notice, however, that there is some debate on the absolute normalization of the data [37]. The soft photon approximation does not so well account for the data. This means that for qualitative analyses of unpolarized bremsstrahlung observables one can use the effective OBE model in a wide energy region from 2 GeV down to the pion threshold.

VI. DISCUSSION AND SUMMARY

The present study of bremsstrahlung in NN reactions relies on the effective OBE model with parameters adjusted to elastic NN scattering. While a generalization of the OBE model to inelastic processes seems straightforward by calculating a considerable number of Feynman diagrams, one also meets not yet satisfactorily clarified items. One such challenging issue concerns the effective strong and electromagnetic form factors.

As mentioned in Section 2 we follow here Ref. [17] and others and neglect the half-off-shell effects in the strong NNM form factors. Since we consider the emission of real photons with $k^2 = 0$ the electromagnetic form factor can still depend on the momentum squared of the virtual nucleon. Desirable would be a unique procedure to introduce off-shell effects in a consistent way for both the strong and the electromagnetic form factors in the general case when the photon has arbitary virtiality, i.e., $k^2 \neq 0$ as in di-electron production and electron scattering. Various aspects of this problem have been studied in Refs. [14,17,22,38,39]. A general outcome seems to be the additional suppression of form factors by off-shell effects.

In summary we report a study of photon production within an effective one-boson exchange model which is indented for a prediction of forthcoming data at COSY-TOF. The present results focus on the general theoretical scheme but compare also successfully with existing data. We mention that accurate data on the elastic scattering and the Δ contributions are needed to get more confidence in the parameters to be employed. It should be stressed that also the reaction $pd \to X\gamma$ is very worth measuring since it provides valuable information on the pn channel.

Acknowledgments: Stimulating discussions with E.L. Bratkovskaya, W. Cassing, H. Freiesleben, E. Grosse, B. & L. Naumann, K. Möller, and U. Mosel are gratefully acknowledged. The work is supported by BMBF grant 06DR829/1 and Heisenberg-Landau foundation.

REFERENCES

[1] D. Grzonka, Nucl. Phys. A 585 (1995) 321
D. Prasuhn et al., Nucl. Instr. and Meth. A 362 (1995) 16
[2] P. Herrmann, Ph.D. thesis, University of Bochum (1997)
[3] F. de Jong, K. Nakayama, T.S.H. Lee, Phys. Rev. C 51 (1995) 2334
[4] V. Herrmann, J. Speth, K. Nakayama, Phys. Rev. C 43 (1991) 394
V. Herrmann, K. Nakayama, Phys. Rev. C 45 (1992) 1450
[5] M. Jetter, H.W. Fearing, Phys. Rev. C 51 (1995) 1666
[6] P. Kitching et al., Phys Rev. Lett. 57 (1986) 2363, Nucl. Phys. A 463 (1987) 87
B. v. Przewoski et al., Phys. Rev. C 45 (1992) 2001
[7] K. Michaelian et al., Phys. Rev. D 41 (1990) 2689
[8] F. de Jong, K. Nakayama, V. Herrmann, O. Scholten, Phys. Lett. B 333 (1994) 1
[9] V. Herrmann, K. Nakayama, O. Scholten, H. Arellano, Nucl. Phys. A 582 (1995) 568
[10] J.A. Eden, M.F. Gari, Phys. Lett. B 347 (1995) 187, preprints RUB-MEP-81/94, 90/95
[11] V.G. Neudatchin, N.A. Khokhlov, A.M. Smirnov, V.A. Knyr, Yad. Fiz. 60 (1997) 1086
[12] B.M.K. Nefkens, O.R. Sander, D.I. Sober, H.W. Fearing, Phys. Rev. C 19 (1979) 877
[13] L. Tiator, H.J. Weber, D. Drechsel, Nucl. Phys. A 306 (1978) 468
[14] B. Kämpfer, A.I. Titov, E.L. Bratkovskaya, Phys. Lett. B 301 (1993) 123
[15] A.I. Titov, B. Kämpfer, E.L. Bratkovskaya, Phys. Rev. C 51 (1995) 227
[16] L.A. Winckelmann, H. Stöcker, W. Greiner, H. Sorge, Phys. Lett. B 298 (1993) 22
K. Haglin, C. Gale, Phys. Rev. C 49 (1994) 401
[17] M. Schäfer, H.C. Dönges, A. Engel, U. Mosel, Nucl. Phys. A 575 (1994) 429
[18] W.K. Wilson et al., Phys. Lett. B 316 (1993) 245
[19] A. Engel, R. Shyam, U. Mosel, A.K. Dutt-Mazumder, Nucl. Phys. A 603 (1996) 387
[20] E.L. Bratkovskaya, W. Cassing, U. Mosel, O.V. Teryaev, A.I. Titov, V.D. Toneev, Phys. Lett. B 362 (1995) 17
[21] A. Szyjewicz, A.N. Kamal, Lecture Notes in Physics 82 (1978) 88, Springer Verlag, Berlin
T.S. Biro, K. Niita, A.L. de Paoli, W. Bauer, W. Cassing, U. Mosel, Nucl. Phys. A 475 (1987) 579
[22] M. Schäfer, T.S. Biro, W. Cassing, U. Mosel, H. Nifenecker, J.A. Pinston, Z. Phys. A 339 (1991) 391
W. Cassing, V. Metag, U. Mosel, K. Niita, Phys. Rep. 188 (1990) 363
M. Schäfer, Ph. D. thesis, Giessen 1994, unpublished
[23] A.I. Titov, B. Kämpfer, B.L. Reznik, V. Shklyar, Phys. Lett. B 372 (1996) 15
[24] R.M. Barnett et al. (Particle Data Group), Phys. Rev. D 54 (1996) 1
[25] K.L. Haglin, Ann. Phys. 212 (1991) 84
[26] I.S. Towner, Phys. Rep. 155 (1987) 263
[27] T. Vetter, A. Engel, T.S. Biro, U. Mosel, Phys. Lett. B 263 (1991) 153
[28] P.J. Carlson et al., in vol. 7, Landolt-Börnstein, Berlin 1973
[29] H. Garcilazo, E. Moya de Guera, Nucl. Phys. A 562 (1993) 521
B. G. Yu, Il-T. Cheon, M. T. Jeon, J. Phys. Soc. Japan 63 (1994) 78
[30] See, for example, SAID user manual (http://CLSAID.PHYS.VT.EDU)
[31] W. Weise, Nucl. Phys. A 278 (1977) 402
V. Dimitriev, O. Sushkov, C. Gaarde, Nucl. Phys. A 459 (1986) 503
[32] B.J. VerWest, R.A. Arndt, Phys. Rev. C 25 (1982) 1979
[33] A.M. Eisner, E.L. Hart, R.I. Louttit, T.W. Morris, Phys. Rev. 138 (1965) B670
[34] Gy. Wolf, W. Cassing, U. Mosel, Nucl. Phys. A 545 (1992) 139

[35] A.L. de Paoli et al., Phys. Lett. B 219 (1989) 194
E. Chiavassa et al., Phys. Lett. B 322 (1994) 270
[36] G.E Brown, W. Weise, Phys. Rep. 22 (1975) 279
[37] V.R. Brown, P.L. Anthony, J. Franklin, Phys. Rev. C 44 (1991) 1296
[38] H.W.L. Naus, J.H. Koch, Phys. Rev. C 36 (1987) 2459
P.C. Tiemeijer, J.A. Tjon, Phys. Rev. C 42 (1990) 599
[39] H.C. Dönges, M. Schäfer, U. Mosel, Phys. Rev. C 51 (1995) 950

TABLE I. The parameter set used in the present work.

meson	mass	coupling	cut-off	energy parameter
M	m_M [GeV]	g_M^0	Λ_M [GeV]	β_M [GeV^{-1}]
π	0.138	11.7	0.75	0.047
ρ	0.770	1.78	1.60	0.047
ω	0.782	9.60	1.23	0.035
σ	0.550	2.03	1.10	0.041

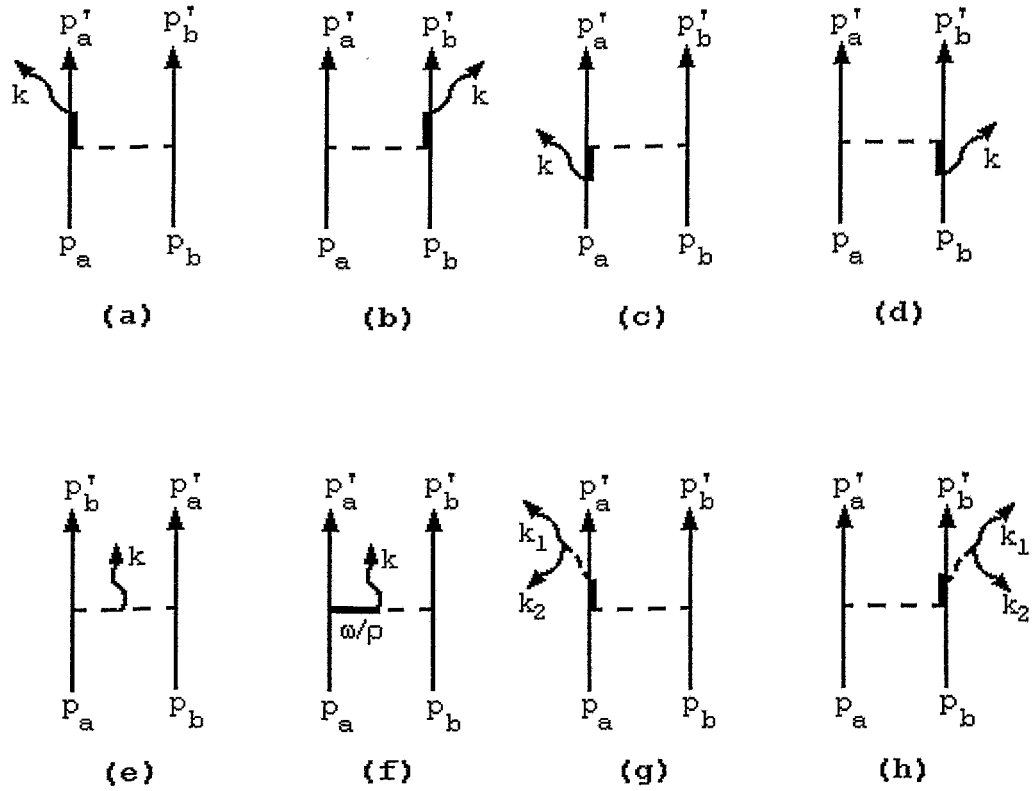

FIG. 1. The Feynman diagrams for NN bremsstrahlung considered in this paper. (a) - (d): bremsstrahlung with an intermediate off-shell nucleon or a Δ (fat lines); (e): photon emission from the exchange of a charged meson, (f): emission from the $V \to \pi\gamma$ transition, i.e., internal radiative meson conversion, (g) and (h): the intermediate nucleon line represents a N_{1535} state which decays into a nucleon and an η, which undergoes subsequent two-photon decay. The exchange digrams are not displayed.

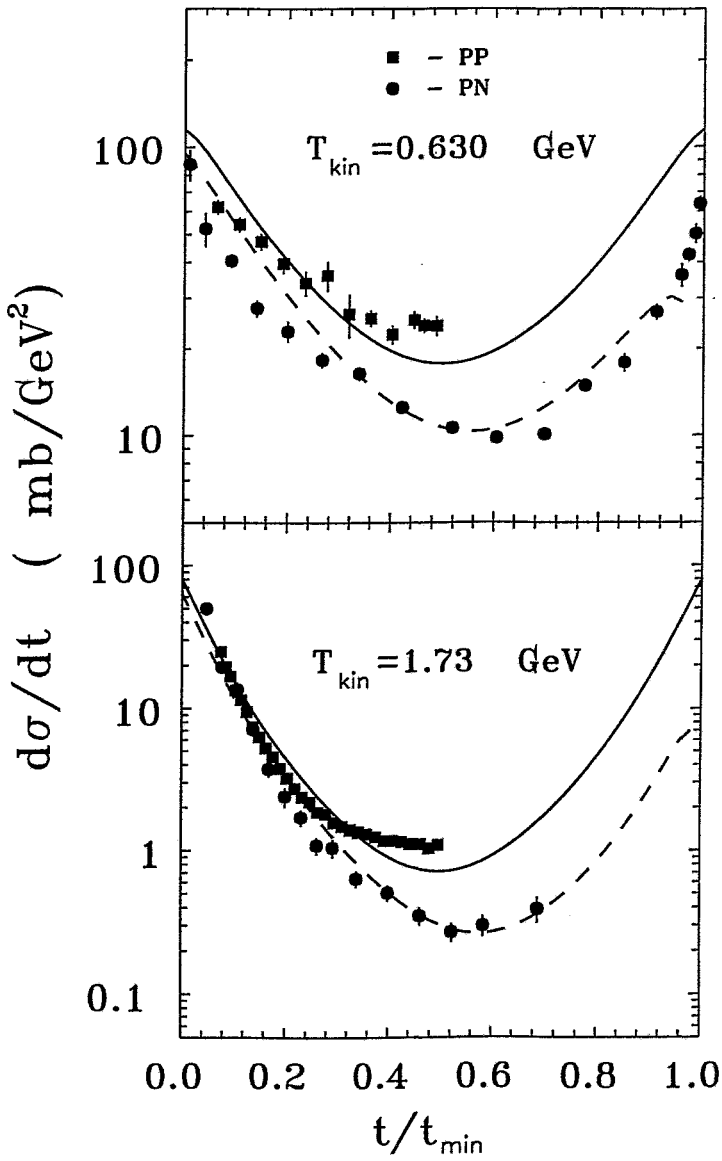

FIG. 2. The elastic nucleon - nucleon cross section at beam energies $T_{\rm kin} = 0.63$ and 1.73 GeV. Solid and dashed lines depict results for the pp an pn reactions. Experimental data are taken from Ref. [28,30]. $t_{\rm min} = 4M_N^2 - s$.

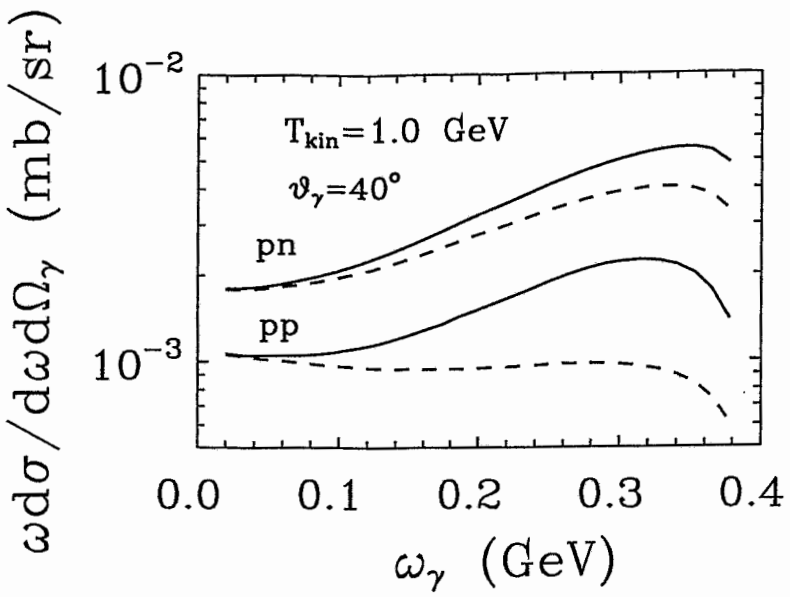

FIG. 3. The differential cross section for proton - proton and proton - neutron bremsstrahlung at $T_{\rm kin}$ = 1 GeV. The cms photon angle is $\vartheta_\gamma = 40^o$. The solid and dashed lines correspond to calculations with and without anomalous magnetic moment contributions.

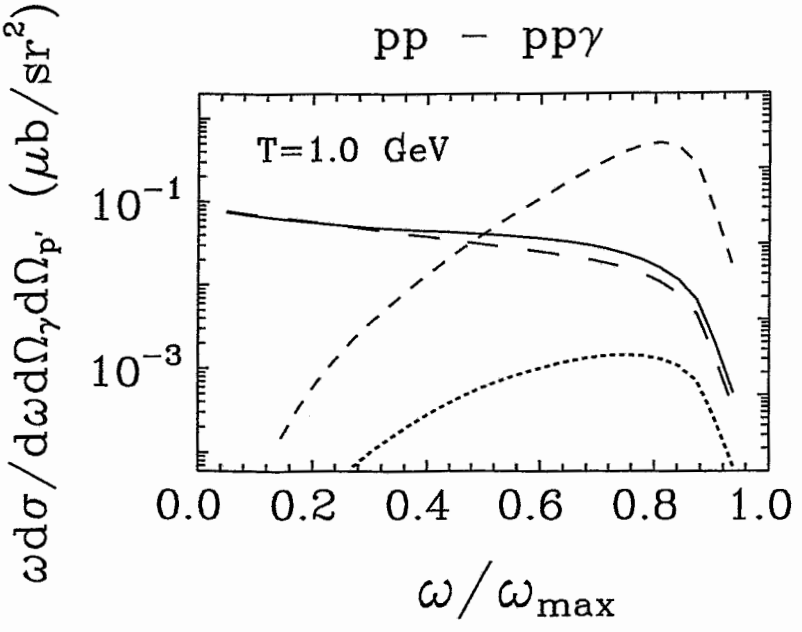

FIG. 4. The radiative meson decay $\omega, \rho \to \pi\gamma$ contribution to the bremsstrahlung at $T_{\rm kin}$ = 1 GeV for fixed angles of the exit particles in cms: $\vartheta_{p'} = 40^o$, $\vartheta_\gamma = 60^o$, $\phi = 60^o$. The solid, short-dashed, long-dashed and dotted curves correspond to the contributions of non-resonance bremsstrahlung, soft photon approximation, Δ decay and ω, ρ decay, respectively.

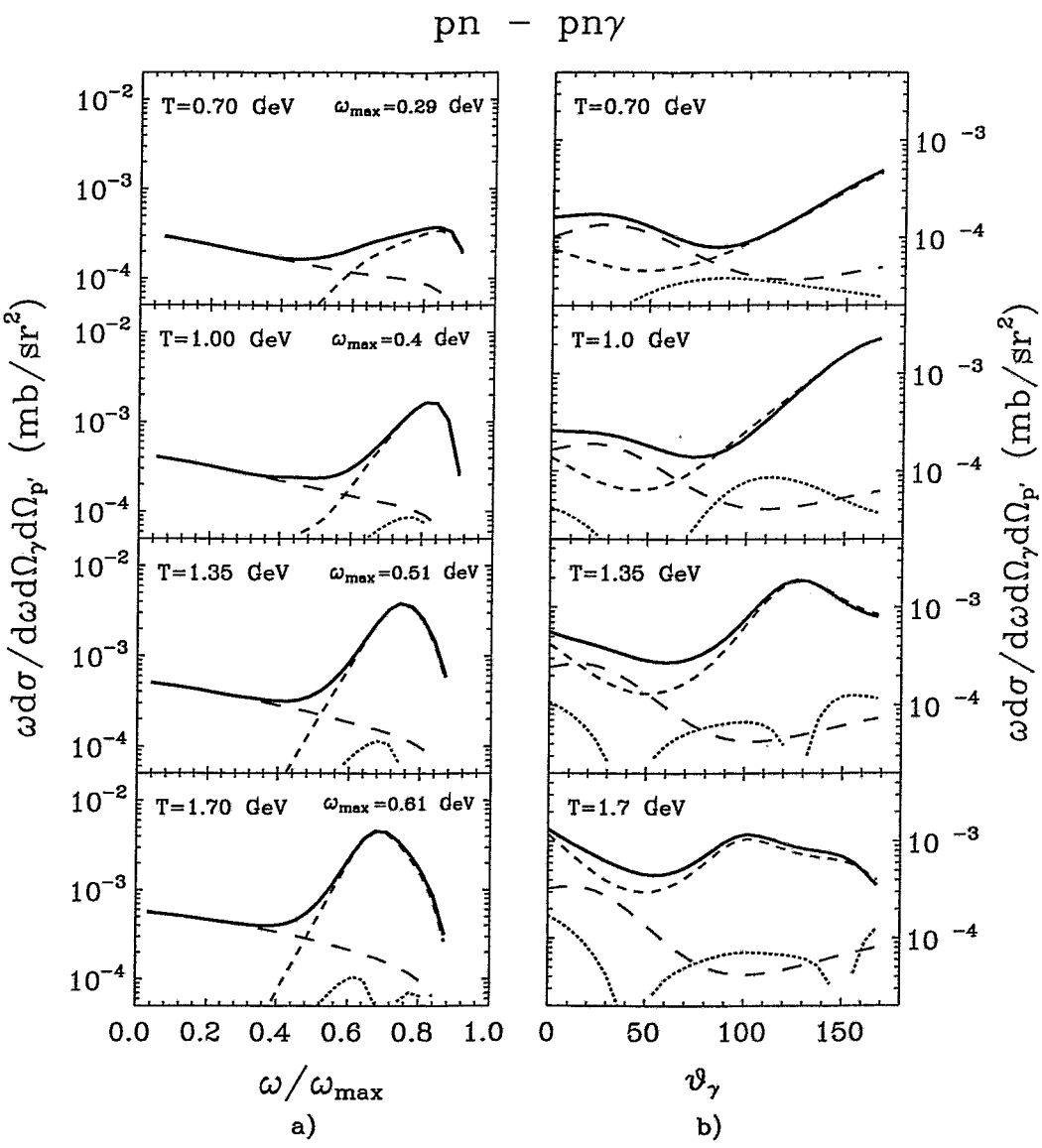

FIG. 5. The differential cross section $\omega d\sigma/d\omega d\Omega_\gamma d\Omega_{p'}$ vs. $\omega/\omega_{\max}$ in cms at $\vartheta_{p'} = 40^o$, $\vartheta_\gamma = 30^o$, $\phi = 60^o$) (a) and vs. ϑ_γ at $\omega/\omega_{\max} = 0.5$ at $\vartheta_{p'} = 40^o$, $\phi = 60^o$ (b) for the reaction $pn \to pn\gamma$ at $T_{\rm kin} = 0.7$, 1.0, 1.35, 1.7 GeV (the meaning of the various lines is the following one: long dashed: bremsstrahlung, short dashed: Δ decay, dotted: interference of bremsstrahlung and Δ decay, heavy solid lines: total cross section).

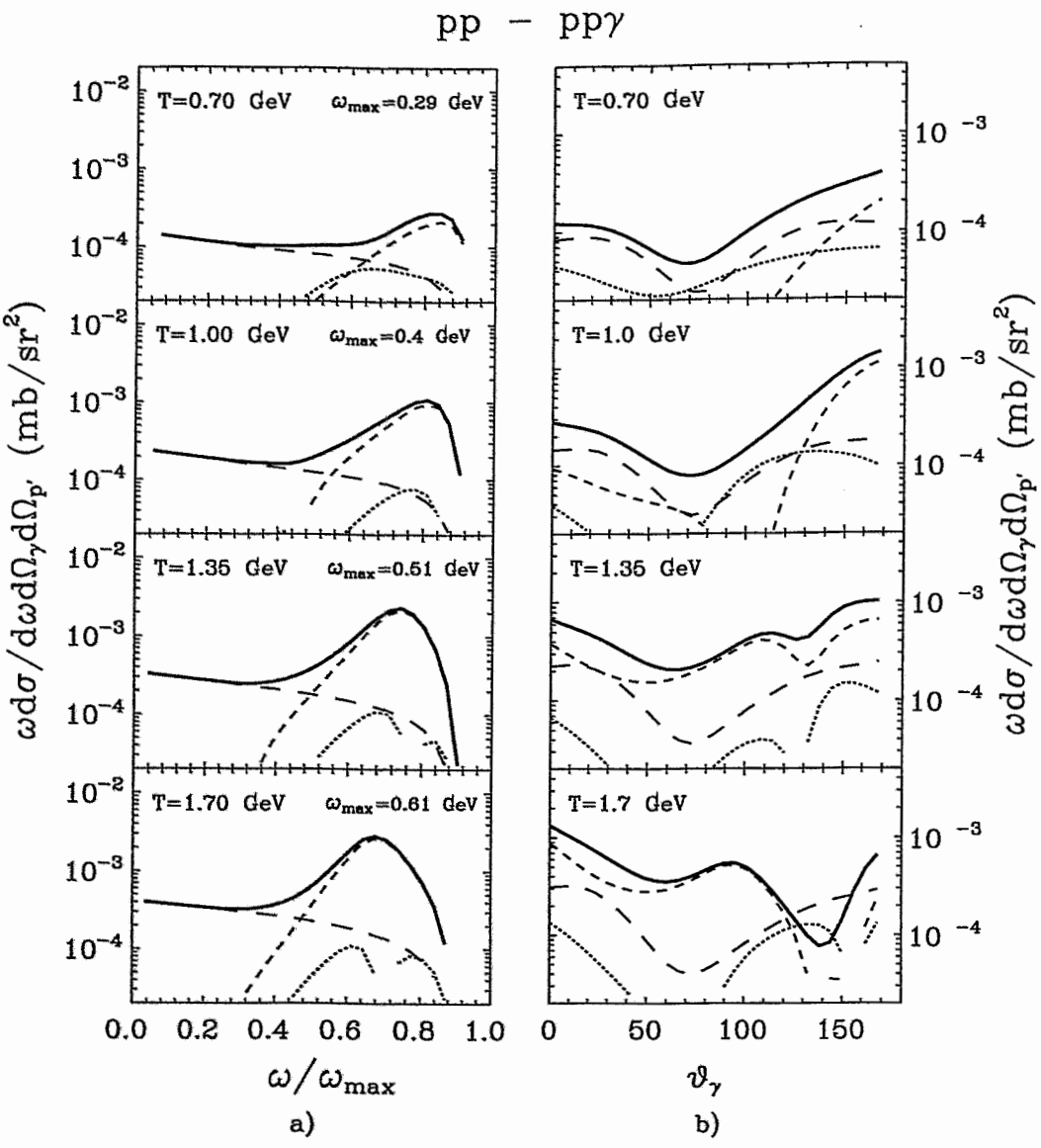

FIG. 6. The same as Fig. 5 but for $pp \to pp\gamma$.

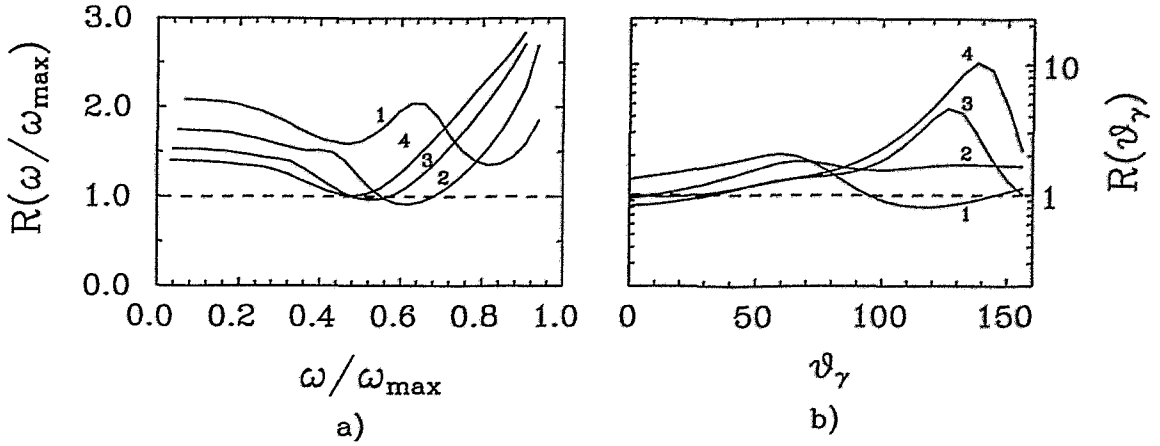

FIG. 7. The ratio $(\omega d\sigma/d\omega d\Omega_\gamma d\Omega_{p'})^{pn}/(\omega d\sigma/d\omega d\Omega_\gamma d\Omega_{p'})^{pp}$ of differential cross sections shown in Figs. 5 and 6 as a function of $\omega/\omega_{\max}$ at $\vartheta_{p'} = 40^o$, $\vartheta_\gamma = 30^o$, $\phi = 60^o$ (a), and as a function of the photon angle at ϑ_γ at $\vartheta_{p'} = 40^o$, $\phi = 60^o$, $\omega/\omega_{\max}$=0.5 (b) for four energies $T_{\rm kin}$=0.7, 1.0, 1.35, 1.7 GeV corresponding to the curves labeled by 1 - 4.

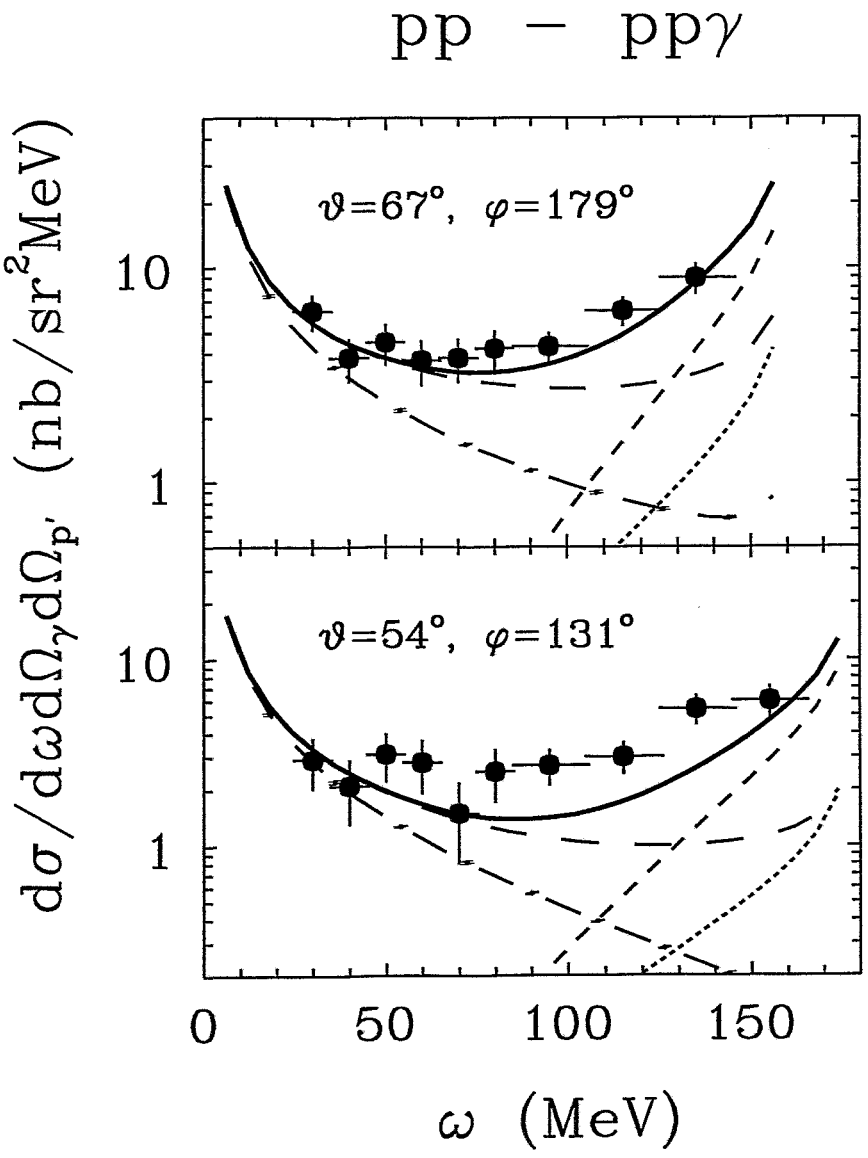

FIG. 8. Comparison of our calculations for the cross section of the real photon production in proton - proton scattering at $T_{\rm kin}$ = 730 MeV with the experimental data for two geometries (counters G07 and G10). The data are taken from the Ref. [12]. Dot-dashed lines: soft photon approximation, long-dashed lines: pure bremsstrahlung, short-dashedlines: Δ decay, dotted lines: Δ - bremsstrahlung interference. The heavy solid curves represent the sum of these contributions.

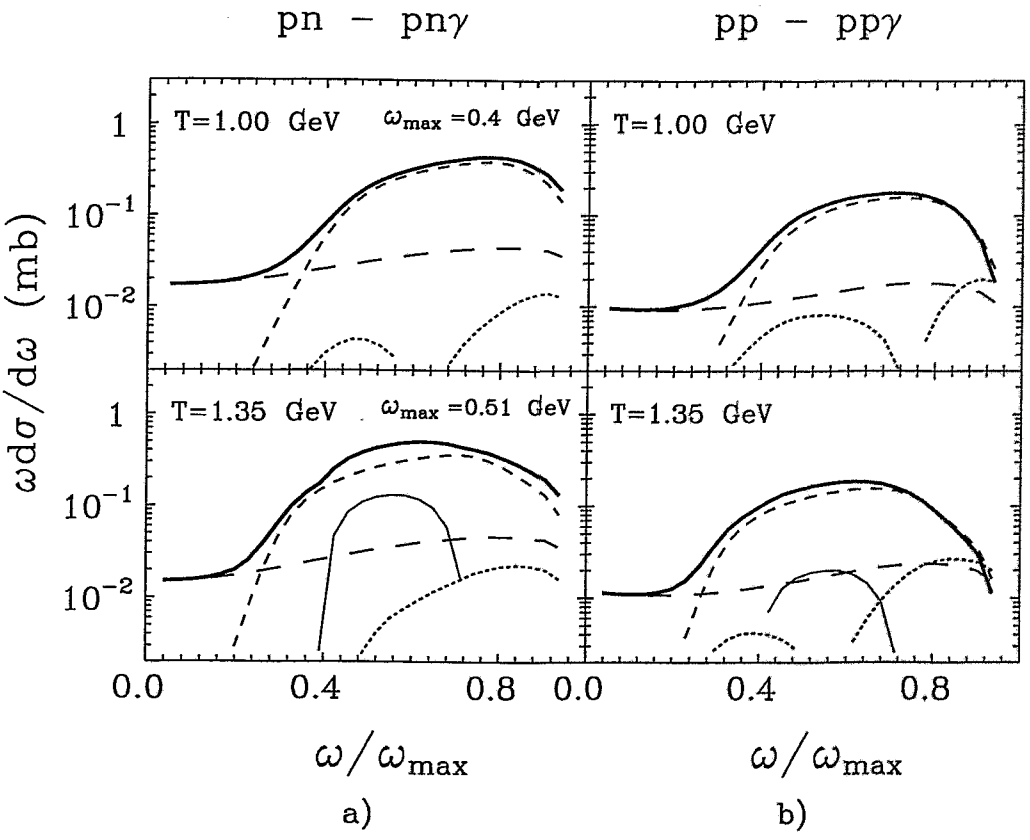

FIG. 9. The differential proton - neutron (a) and proton - proton (b) cross sections in cms as a function of the photon energy for illustrating the η decay contribution to the photon production in comparison with others channels at two beam energies $T_{\rm kin}$ = 1.0 and 1.35 GeV. The long-dashed, short-dashed, dotted and solid lines represent pure bremsstrahlung, Δ decay, Δ decay - bremsstrahlung interference, and η decay. The heavy solids curve show the sum of these contributions.

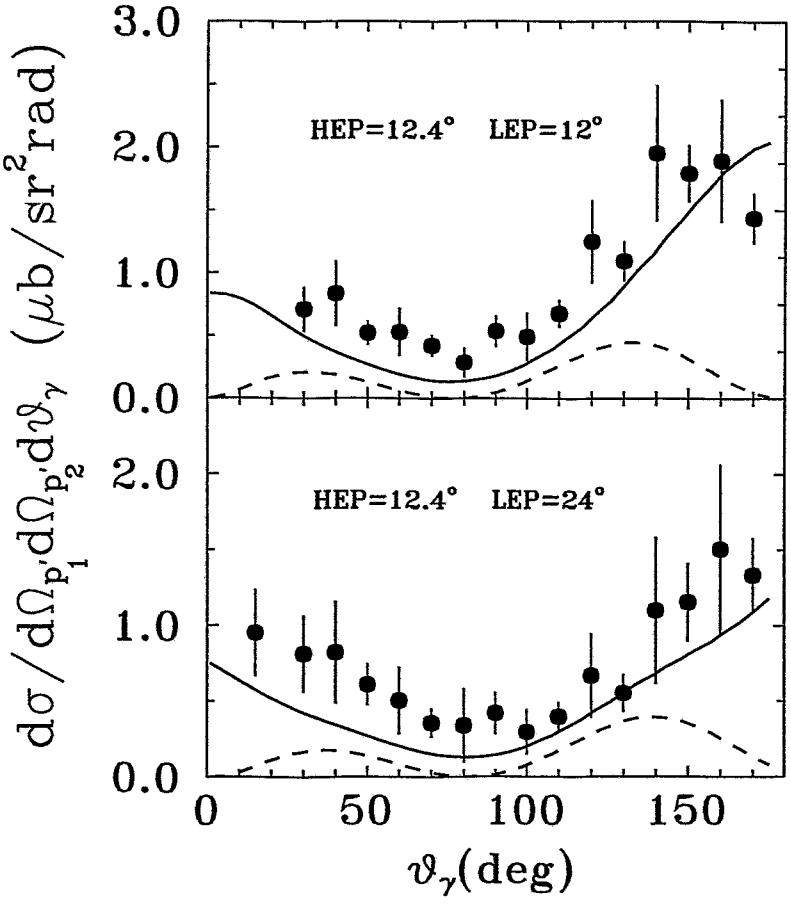

FIG. 10. Comparison of our calculations for the $pp \to pp\gamma$ cross section with experimental data at beam energy $T_{\rm kin} = 280$ MeV. The data are taken from Ref. [7] and scaled by a factor 2/3 as discussed in Ref. [37]. The solid and dashed lines represent a pure bremsstrahlung calculation and soft photon approximation. The notion of HEP and LEP angles correspond to high-energy and low-energy protons respectively.